Experimental generation of Mathieu–Gauss beams with a phase-only spatial light modulator

R. J. Hernández-Hernández,[1] R. A. Terborg,[1] I. Ricardez-Vargas,[1,2] and K. Volke-Sepúlveda[1,*]

[1]Instituto de Física, UNAM, Apdo. Postal 20-364, 01000 México D.F., México

[2]Universidad Politécnica del Centro, 86291 Centro, Tabasco, México

*Corresponding author: karen@fisica.unam.mx

We present a novel method for the efficient generation of even, odd, and helical Mathieu–Gauss beams of arbitrary order and ellipticity by means of a phase-only spatial light modulator (SLM). Our method consists of displaying the phase of the desired beam in the SLM; the reconstructed field is obtained *on-axis* following a spatial filtering process with an annular aperture. The propagation invariance and topological properties of the generated beams are investigated numerically and experimentally.   © 2010 Optical Society of America

OCIS codes: 070.3185, 090.1995, 070.6120, 120.5060.

1. Introduction

Propagation invariant optical fields (PIOFs) are solutions of the wave equation in cylindrical coordinate systems with different geometries in the transverse plane; their name is owed to the fact that their transverse intensity profile is independent of the axial propagation coordinate z. There are four families of PIOFs; each one of them constitutes a complete orthogonal basis in terms of which any arbitrary light beam can be expanded. The best-known member of these families is the plane wave and, in the context of PIOFs, some particular combinations thereof whose transverse intensity profiles form stationary waves along the x and/or the y directions, such as $\{\cos k_t x, \cos k_t y\}$. On the other hand, Bessel beams correspond to the case of circular cylindrical geometry and were introduced in 1987 by Durnin *et al.* [1]. Mathieu beams, brought in by Gutierrez-Vega *et al.* [2] in 2001, are associated with elliptic transverse geometry, but in fact, they can also be associated with hyperbolic geometry, since the elliptical cylindrical coordinate system is formed by orthogonal families of confocal elliptic and hyperbolic cylinders that intersect each other [3]. Finally, parabolic PIOFs were introduced in 2004 by the latter group [4]. There are also different vector families of PIOFs, which satisfy the vector wave equation [5,6]. PIOFs share several properties, for example, their wave vectors lie on the surface of a cone with axial and transverse components denoted here by k_z and k_t, respectively [7]. In consequence, the Fourier spectrum of any PIOF is constituted by a single ring of radius k_t in the frequency domain; the amplitude and phase modulation around this ring defines each particular PIOF [2,4]. Another characteristic shared by all the PIOFs is that they, in principle, carry infinite energy just as is commonly accepted with the plane wave, and therefore, ideal PIOFs are not realizable in the laboratory. In this context, finite versions of the ideal PIOFs known as Bessel–Gauss beams in the case of circular geometry [8], and more recently designated as Helmholtz–Gauss waves in general, have been studied [9]. In this paper, we focus our attention on Mathieu–Gauss beams, which are also a special case of the so-called elliptical beams [10].

Mathieu beams and Mathieu–Gauss (MG) beams have been the focus of considerable attention in

the last few years because their topological properties depend on the interfocal distance $2f$. This parameter provides elliptic light beams with richness that their circular and rectangular counterparts do not possess. In the limit when $f = 0$, one recovers the case of circular geometry and Mathieu beams transform into Bessel beams. The tailoring of topological properties of Mathieu beams has found relevant applications in nonlinear optics. For instance, it has been found that a variation of f from 0 to ∞ can be used for shaping solitons in Mathieu lattices of the lowest order [11].

In circular geometry, the even and odd solutions of the wave equation, $J_m(k_t\rho)\cos m\varphi$ and $J_m(k_t\rho)\sin m\varphi$, respectively, are degenerate with respect to the eigenvalue m. This allows a straightforward construction of complex superpositions that give rise to rotating modes called optical vortices, with azimuthal phase dependence of the form $\{\exp(\pm im\varphi)\}$, where the eigenvalue m is known as the topological charge of the vortex. Optical vortices are highly relevant in optics, not only due to their topological properties, as they exhibit a screw-type singularity [12], but also due to their dynamical properties. They possess a well-defined orbital angular momentum [13,14]. Both characteristics have led to a great number of applications [15–20]. In elliptic coordinates, in contrast, the eigenvalues of even and odd solutions of the wave equation are different; the larger the interfocal distance f, the more the eigenvalues differ from one another. Nevertheless, complex superpositions of even and odd Mathieu beams that are analogous to Bessel vortices have been proposed for generating what has been called elliptic vortices [21] or helical Mathieu (HM) beams, which have been used, for instance, for rotating microscopic particles [22]. In nonlinear optics, theoretical predictions show that HM lattices support stable solitons that may either oscillate or rotate around an elliptical ring of the lattice as they propagate, provided the launched field initially possesses a transverse linear momentum component tangent to the lattice ring [23]. Elliptic vortices may be supported as well in HM lattices whenever the energy flow exceeds certain minimum value, in contrast with circular vortices [24]. Recently, the dynamical effects of vector Mathieu beams on cold atoms trapped in a far-off resonance optical trap were investigated [25]. In that case, the Mathieu modes were characterized by a single eigenvalue, which allowed the identification of a new dynamical constant associated with elliptical symmetry, analogous to the orbital angular momentum in circular geometry.

In spite of the increasing attention that Mathieu and MG beams have recently received in connection with new proposed applications, there are just few reports on the experimental generation of these kinds of beams [26–28]. The first experimental demonstration was limited to the lowest order Mathieu beam [26]. The second approach was based on phase-only computer generated holograms (CGH), for which the produced MG beams of arbitrary order and ellipticity are reconstructed off-axis, giving rise to a relatively low efficiency [27]. Finally, all the families of Helmholtz–Gauss beams, including MG modes, were generated experimentally by means of Fourier CGHs, which are computed as the interference pattern between the interest field and an inclined plane wave [28]. The latter approach produces good quality beams, but the efficiency is lower than that obtained with the phase holograms.

In this article, we present a versatile method for the generation of Mathieu–Gauss beams of arbitrary order and ellipticity by using a phase spatial light modulator (SLM). Our code is simple and more efficient than its predecessors, since the structured light beams are generated on-axis. It consists in displaying the phase of the desired beam in the SLM and making a spatial filtering process with an annular aperture. In Section 2, we present a numerical analysis of our system for the generation of even, odd, and helical MG modes. The experimental setup and results are discussed in Section 3, including a characterization of the propagation and topological properties of the generated light fields. Section 4 is dedicated to the conclusions.

2. Numerical Analysis

The generation of Bessel beams (BBs) by means of digital holography was accomplished shortly after these optical fields were introduced [29]. Similar encoding techniques were implemented some years later using spatial light modulators [30], with the significant advantage offered by the dynamical reconfiguration. However, in most of these methods the encoded fields are reconstructed off-axis, which gives rise to relatively low efficiencies. Very recently, a new encoding technique was introduced for generating BBs with a phase-only SLM, which dramatically improves the output power efficiency [31,32]. Here we follow the same method: the phase of the *ideal* nondiffracting beam of interest is displayed on the SLM and the field is reconstructed *on-axis*. As we illuminate the SLM with a fundamental Gaussian beam, the resulting field is a Mathieu–Gauss beam.

The phase masks we displayed for the generation of even, odd, and helical Mathieu beams of order r can be expressed, respectively, as

$$M_r^e(u,v) = \operatorname{sgn}\{ce_r(v;q)Je_r(u;q)\}, \tag{1}$$

$$M_r^o(u,v) = \operatorname{sgn}\{se_r(v;q)Jo_r(u;q)\}, \tag{2}$$

$$M_r^h(u,v) = \exp\left\{\pm i \arctan\left(\frac{A_r(q)ce_r(v;k_t,q)Je_r(u;k_t,q)}{B_r(q)se_r(v;k_t,q)Jo_r(u;k_t,q)}\right)\right\}. \tag{3}$$

We have followed here the notation used in Ref. [2], where $ce_r(v;q)$ and $se_r(v;q)$ represent the even and

odd ordinary Mathieu functions, also known as elliptic cosine and sine, respectively, while $Je_r(u; q)$ and $Jo_r(u; q)$ denote the even and odd modified Mathieu functions. The ellipticity parameter is defined as $q = f^2 k_t^2/4$, and the elliptic transverse coordinates (u, v) are related with the Cartesian coordinates (x, y) by means of the transformation $x = f \cosh u \cos v$; $y = f \sinh u \sin v$. In Eqs. (1) and (2), sgn$\{\cdot\}$ represents the binary signum function. Its two possible values are mapped to phase values of 0 and π in our SLM display. The coefficients $A_r(q)$ and $B_r(q)$ in Eq. (3) are defined according to Ref. [21]. In our numerical analysis, we multiply each of the above functions by a Gaussian amplitude of radius w_0, $G_0 = \exp(-\rho^2/w_0^2)$, and this constitutes our initial condition at the plane $z = 0$. We study the generated optical field by means of standard Fresnel propagation algorithms. The field is propagated through a conventional $4f$ system, consisting of two lenses of focal length f_L and an annular aperture filter at the Fourier plane.

Figures 1 and 2 show simulations of the optical fields generated with phase masks corresponding, respectively, to an even Mathieu beam of order $r = 6$ and ellipticity parameter $q = 18$ and a helical Mathieu beam of order $r = 6$ and ellipticity parameter $q = 12$. In both cases, the transverse spatial frequency is $k_t = 10$ mm^{-1}. In each of the figures, we show the transverse optical field at different planes z (a–e), the phase mask (f), and the resulting field along the propagation axis (g). The axial distance z has been scaled respect to the focal length f_L and the transverse coordinates (x, y) with respect to the beam waist w_0. In order to facilitate the visualization of the Fourier spectrum (FS), the wavelength

was taken sufficiently large ($\lambda = 0.05$ mm), which means that the real spectrum will be 100 times smaller for a wavelength of 500 nm, for instance. The FS in both cases consists of a main ring in which most of the energy is concentrated and has additional surrounding structure of much lower energy. The radius and width of the annular filter at the Fourier plane were set in order to allow the transmission of the light from the main ring, while blocking the rest. It has been demonstrated that the FS of any Helmholtz–Gauss beam is constituted by a single ring whose mean radius in the frequency domain is k_t, which is associated with the FS of the corresponding ideal PIOF, and whose width is associated with the Gaussian envelope [9]. Accordingly, we have set the radius and width of the annular filter as $R = k_t \lambda f_L/2\pi$ and $\Delta R = 2\lambda f_L/w_0\pi$, respectively.

The generated MG beams are approximations to ideal Mathieu nondiffracting beams within a certain region of space, since their transverse intensity profiles remain approximately unaltered along this region. The propagation invariance distance is directly proportional to the radius of the Gaussian envelope [9,32]. In the case of helical MG beams, there is an additional effect arising from the finite size of the Gaussian modulation. Consider, for example, the helical MG beam shown in Fig. 2(d), whose transverse intensity distribution has a set of $r = 6$ vortices with unit topological charge lined up along the major axis of the ellipse [21]. From a comparison with Figs. 2(c) and 2(e), it can be seen that the line of vortices exhibits a slight rotation on propagation. This behavior was predicted and observed for corotating vortices nested in a Gaussian beam [33], and it has been also observed in the specific case of helical MG
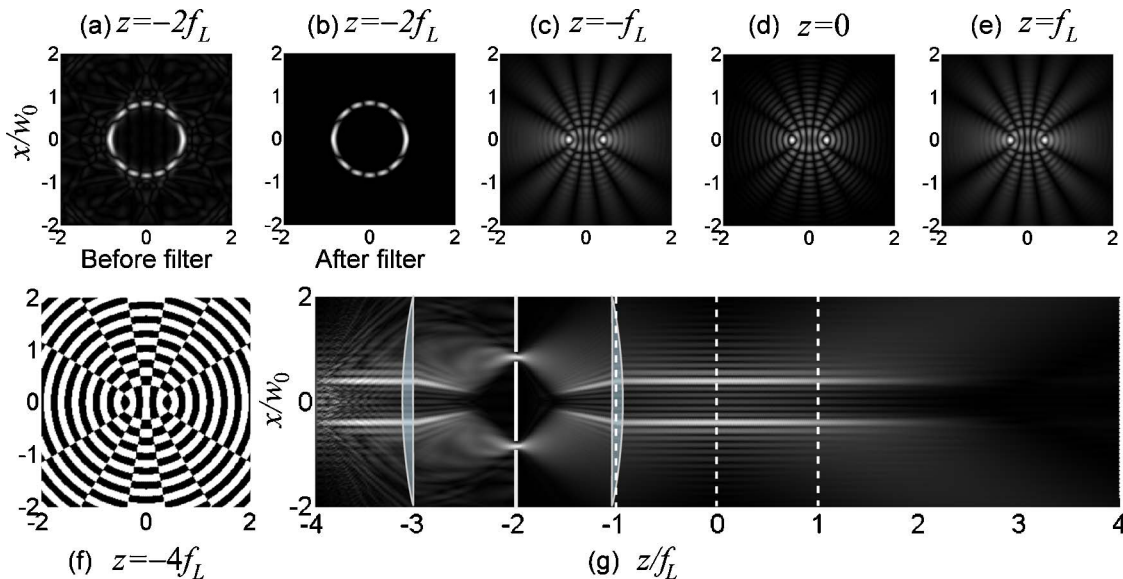

Fig. 1. (Color online) Simulation of the propagation of an input Gaussian beam impinging on a phase mask located at $z = -4f_L$ encoding the phase of an even Mathieu beam of order $r = 6$ and ellipticity parameter $q = 18$. (a), (b) Fourier spectrum just before and after the annular screen. (c)–(e) Transverse intensity distribution of the reconstructed field at different planes. (f) Phase mask. (g) Axial intensity distribution along propagation through the $4f$ optical system. The dashed lines indicate the planes where the transverse profiles (c)–(e) were taken. The phase in the mask varies from 0 to π.
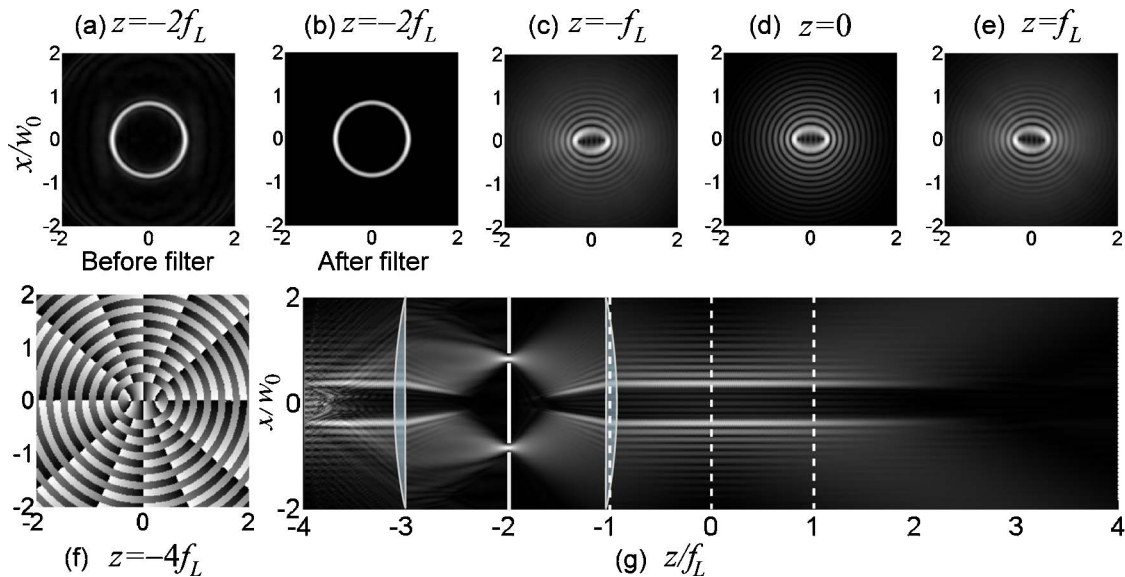
Fig. 2. (Color online) Same as Fig. 1, for a phase mask encoding a helical Mathieu beam of order $r = 6$ and ellipticity parameter $q = 12$. The phase in the mask varies from 0 to 2π.

beams [27]. Ideal nondiffracting Mathieu beams would not exhibit this rotation. Therefore, this effect can be minimized by enlarging the Gaussian envelope.

The output power efficiency of the optical fields generated with the proposed phase masks, calculated as the ratio of the power remaining after the annular filter to the incident power, can be as high as ~80%, but it depends on the involved parameters. Specifically, the efficiency decreases as a function of the ellipticity parameter q, for instance, for $r = 3$, $k_t = 10$ mm^{-1} and $w_0 = 2.35$ mm, it drops from 76% when $q = 1$ to 63% when $q = 80$. Regarding the beam order r, we found that the efficiency can drop from 77% to 28% for $r = 5$ and $r = 20$, respectively, for $q = 20$, $k_t = 10$ mm^{-1} and $w_0 = 2.35$ mm. We also found that the efficiency depends strongly on the beam waist of the Gaussian envelope w_0. As an example, it drops from 77% when $w_0 = 2.35$ mm down to 30% when w_0 is five times larger. According to this last result, we infer that the light diffracted from the central region of the mask has a more important contribution to the main ring of the FS than the light coming from the outer region. Finally, we found that k_t does not have an important effect on the efficiency, although this is an important parameter in terms of the pixel structure of an SLM. A larger value for k_t implies smaller details to be resolved with the SLM.

It is worth pointing out that our numerical analysis is based on ideal conditions, while in practice, there are several effects that may considerably deteriorate the efficiency and performance of the phase masks displayed in the SLM. For instance, the partial specular reflection at the front surface of the SLM contributes with unmodulated light traveling on-axis, and there is an additional widespread diffraction pattern associated with the pixel structure

of the SLM. Both of these contributions are ruled out by means of the spatial filtering process, but they may decrease the efficiency by approximately 8% to 15%. Furthermore, another issue that can significantly affect the quality of the generated field is a curvature exhibited by many SLM chips, which sometimes demands a correction of the phase masks. This fact may become more important if the transverse size of the generated beams is reduced down to characteristic dimensions on the order of microns. In our experiments, the transverse size of the generated fields was relatively large; we did not note any distortion due to a curvature of the SLM chip.

3. Experiment and Results

In this work, we use a reflection spatial phase modulator (Holoeye LC-R-2500). The experimental setup for the generation of Mathieu beams corresponds to a conventional $4f$ spatial filtering system (Fig. 3). A
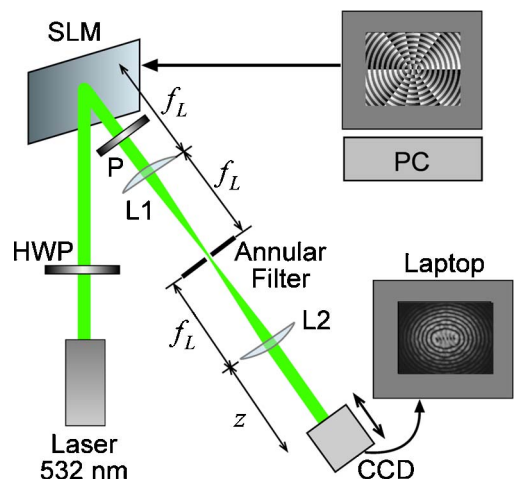

Fig. 3. (Color online) Experimental setup. HWP, half-wave plate; SLM, spatial light modulator; P, polarizer; L, lenses; CCD, camera.

continuous wave linearly polarized laser beam (wavelength, 532 nm) passes through a half-wave plate (HWP) and impinges on the SLM with an angle of approximately $\pi/15$, the minimum allowed by our optical mounts. The fast axis of the HWP and the transmission axis of a linear polarizer P, placed after the SLM, are oriented in such way that the performance of the SLM is optimized. In our case, the lenses L1 and L2 have focal lengths of 25 cm and, as discussed above, the spatial filtering is performed by means of an annular aperture.

In Fig. 4, we present examples of the experimental results for different MG beams (left column) and their corresponding Fourier spectra at the far field (right column). From top to bottom, the images correspond to even, odd, and helical MG beams with $r = 6$ and $q = 12$. Figure 5 shows two sets of images illustrating the propagation invariance for two examples of the generated light beams. Specifically, the left column corresponds to an even MG beam with $r = 3$ and $q = 12$, while the right column illustrate the case of an odd MG mode of order $r = 16$ and $q = 18$. The transverse plane with the best field reconstruction is the back focal plane of the second lens, which was set here as $z = 0$. The waist of the incident beam was relatively small: $w_0 = 2.35$ mm, giving rise to a correspondingly short propagation invariance distance of approximately 50 cm.

In order to characterize the topological properties of the helical MG beams, we used two different methods: direct interference with a plane wave, and the knife-edge probe [34], illustrated in Figs. 6 and 7, respectively. In Fig. 6, we analyzed two cases of helical MG beams: (a)–(d) $r = 6$ and $q = 18$ and (e)–(h) $r = 3$ and $q = 12$. The left column corresponds to simulations and the right column, to experimental results. A number of two-pronged fork-like patterns can be clearly identified along the focal line of each of the two beams. Each two-pronged fork is the fingerprint of the interference between a single-charged vortex and a plane wave [33]. In this way, we can see that each of the two helical MG beams has a set of r individual single-charged vortices. The sets of forks are inverted in (c)–(d) with respect to (g)–(h), because the two beams we are characterizing rotate in opposite directions, which means that the
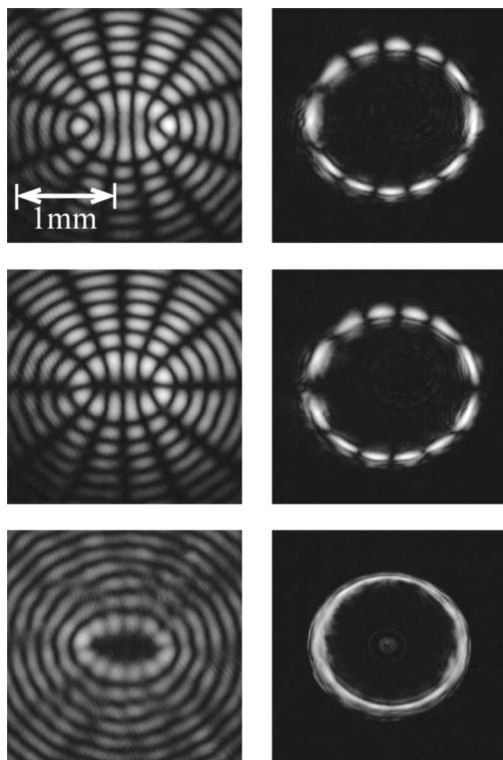

Fig. 4. Experimental images of Mathieu–Gauss beams with $r = 6$ and $q = 12$ (left) and their corresponding Fourier spectra (right). From top to bottom: even MG beam, odd MG beam, and helical MG beam.
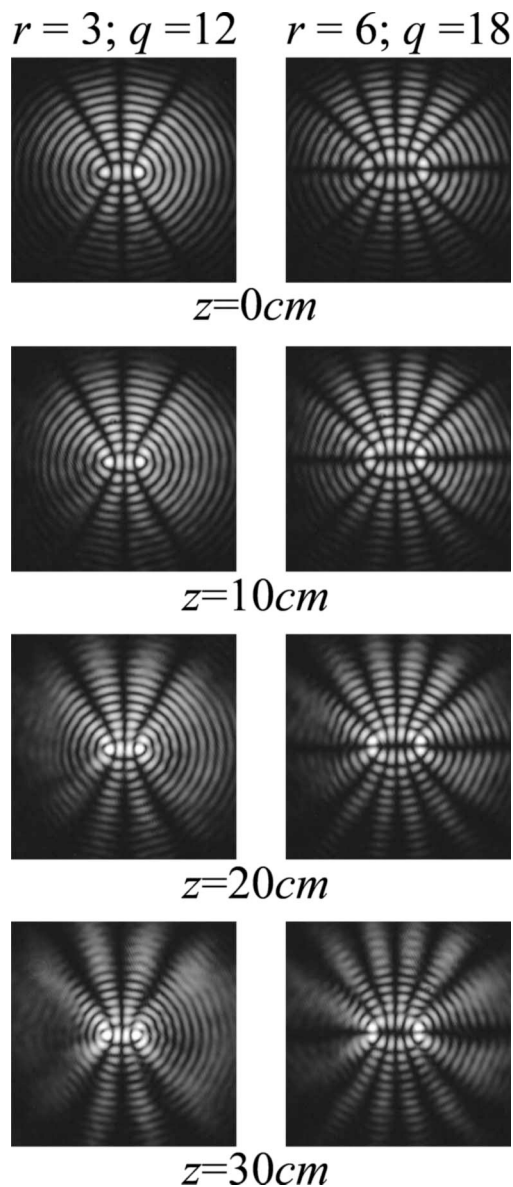

Fig. 5. Test of the propagation invariance of the generated optical fields. Left column: even MG beam with $r = 3$ and $q = 12$. Right column: odd MG beam with $r = 6$ and $q = 18$. The plane $z = 0$ corresponds to the back focal plane of the second lens in the $4f$ system.
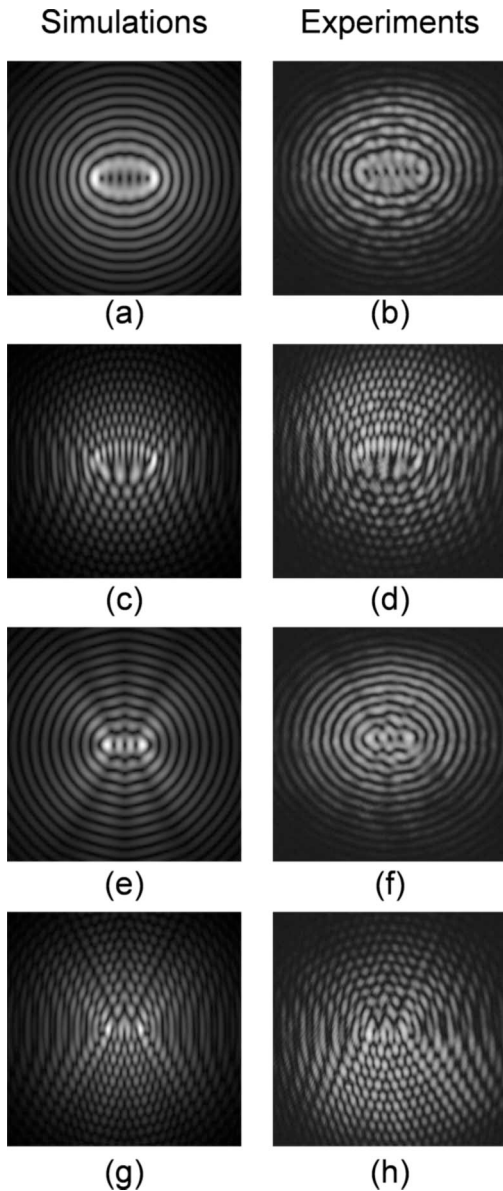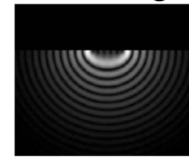
Fig. 6. Numerical simulations (left column) and experimental results (right column) of the transverse intensity distribution of two helical Mathieu–Gauss beams and their interference patterns with a plane wave propagating at a small angle relative to each other. (a)–(d) $r = 6$ and $q = 18$, (e)–(h) $r = 3$ and $q = 12$.

corresponding phase masks have opposite signs in the phase term of Eq. (3). In addition, there is a π-phase shift between consecutive rings of the beam, which can be noted from the shift of the interference fringes. Finally, Fig. 7 illustrates the results of the knife-edge probe for a helical MG beam with $r = 6$ and $q = 12$. Figure 7(a) is a simulation showing the knife edge obstructing the beam at the back focal plane of the second lens. In Fig. 7(b), we show simulations (left) and experimental images (right) when the CCD camera is placed at a distance of 10 cm from the knife edge. The top and bottom rows correspond to helical beams rotating in opposite directions. It is seen that the diffraction pattern spreads asymmetrically in both cases, but the asymmetry is opposite.
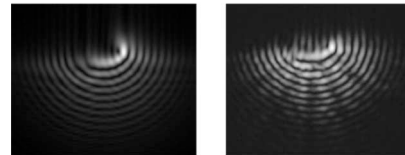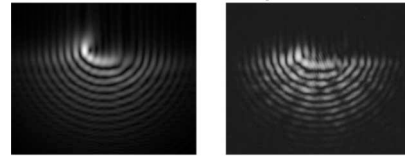
Fig. 7. Knife-edge test for helical Mathieu–Gauss beams with $r = 6$ and $q = 12$. (a) Simulation of the knife edge obstructing the beam at the plane $z = 0$. (b) Numerical simulations (left) and experimental results (right) at the plane $z = 10$ cm from the knife edge. The top and bottom rows correspond to helical beams rotating in opposite directions.

This is an indicative of the rotating energy flux in the case of beams with a helical phase [34].

4. Conclusions

We have proposed a simple and efficient experimental scheme for generating Mathieu–Gauss beams of arbitrary order and ellipticity using a spatial light modulator. Our scheme is based on the display of phase masks in the SLM, which correspond to the phase of the ideal Mathieu beams. The generated fields are filtered by means of an annular aperture whose dimensions (radius and width) are determined by the calculated Fourier spectrum of the light beam of interest. We verified that the resultant optical fields are propagation invariant over a distance, in our case of tens of centimeters, which is in agreement with the simulations, according to the size of the incident light beam. We also analyzed the phase behavior or topological properties of the different light fields by means of direct interference with a plane wave and also by determining the energy flux direction with the knife-edge test [34]. We offer, in this way, a simple tool for implementing new experiments involving Mathieu beams, such as the interesting systems studied recently from a theoretical perspective [11,23–25]. The same method can be employed for the generation of other kinds of optical fields, such as parabolic nondiffracting beams [4].

References

1. J. Durnin, J. J. Miceli, and J. H. Eberly, "Diffraction-free beams," Phys. Rev. Lett. **58**, 1499–1501 (1987).
2. J. C. Gutiérrez-Vega, M. D. Iturbe-Castillo, and S. Chávez-Cerda, "Alternative formulation for invariant optical fields: Mathieu beams," Opt. Lett. **25**, 1493–1495 (2000).
3. P. M. Morse and H. Feshbach, *Methods of Theoretical Physics* (McGraw-Hill, 1953), p. 657.
4. M. A. Bandres, J. C. Gutiérrez-Vega, and S. Chávez-Cerda, "Parabolic nondiffracting optical wave fields," Opt. Lett. **29**, 44–46 (2004).
5. Z. Bouchal and M. Olivik, "Non-diffractive vector Bessel beams," J. Mod. Opt. **42**, 1555–1566 (1995).
6. K. Volke-Sepúlveda and E. Ley-Koo, "General construction and connections of vector propagation invariant optical fields: TE and TM modes and polarization states," J. Opt. A Pure Appl. Opt. **8**, 867–877 (2006).
7. J. Turunen and A. T. Friberg, "Self-imaging and propagation-invariance in electromagnetic fields," Pure Appl. Opt. **2**, 51–60 (1993).
8. F. Gori, G. Guattari, and C. Padovani, "Bessel-Gauss beams," Opt. Commun. **64**, 491–495 (1987).
9. J. C. Gutiérrez-Vega and M. A. Bandres, "Helmholtz—Gauss waves," J. Opt. Soc. Am. A **22**, 289–298 (2005).
10. M. A. Bandres and J. C. Gutiérrez-Vega, "Elliptical beams," Opt. Express **16**, 21087–21092 (2008).
11. Yaroslav V. Kartashov, Alexey A. Egorov, Victor A. Vysloukh, and Lluis Torner, "Shaping soliton properties in Mathieu lattices," Opt. Lett. **31**, 238–240 (2006).
12. J. F. Nye and M. V. Berry, "Dislocations in wave trains," Proc. R. Soc. A **336**, 165–190 (1974).
13. L. Allen, M. W. Beijersbergen, R. J. C. Spreeuw, and J. P. Woerdman, "Orbital angular momentum of light and the transformation of Laguerre–Gaussian laser modes," Phys. Rev. A **45**, 8185–8189 (1992).
14. K. Volke-Sepúlveda, V. Garcés-Chávez, S. Chávez-Cerda, J. Arlt, and K. Dholakia, "Orbital angular momentum of a high-order Bessel light beam," J. Opt. B Quant. Semiclass. Opt. **4**, S82–S88 (2002).
15. H. He, M. E. J. Friese, N. R. Heckenberg, and H. Rubinsztein-Dunlop, "Direct observation of transfer of angular momentum to absorptive particles from a laser beam with a phase singularity," Phys. Rev. Lett. **75**, 826–829 (1995).
16. J. W. R. Tabosa and D. V. Petrov, "Optical pumping of orbital angular momentum of light in cold cesium atoms," Phys. Rev. Lett. **83**, 4967–4970 (1999).
17. V. Garcés-Chávez, K. Volke-Sepúlveda, S. Chávez-Cerda, W. Sibbett, and K. Dholakia, "Orbital angular momentum transfer to an optically trapped low-index particle," Phys. Rev. A **66**, 063402 (2002).
18. D. McGloin and K. Dholakia, "Bessel beams: diffraction in a new light," Contemp. Phys. **46**, 15–28 (2005).
19. M. F. Andersen, C. Ryu, P. Clade, V. Natarajan, A. Vaziri, K. Helmerson, and W. D. Phillips, "Quantized rotation of atoms from photons with orbital angular momentum," Phys. Rev. Lett. **97**, 170406 (2006).
20. R. Pugatch, M. Shuker, O. Firstenberg, A. Ron, and N. Davidson, "Topological stability of stored optical vortices," Phys. Rev. Lett. **98**, 203601 (2007).
21. S. Chávez-Cerda, J. C. Gutiérrez-Vega, and G. H. C. New, "Elliptic vortices of electromagnetic wave fields," Opt. Lett. **26**, 1803–1805 (2001).
22. C. López-Mariscal, J. C. Gutiérrez-Vega, G. Milne, and K. Dholakia, "Orbital angular momentum transfer in helical Mathieu beams," Opt. Express **14**, 4182–4187 (2006).
23. A. Ruelas, S. Lopez-Aguayo, and J. C. Gutiérrez-Vega, "Stable solitons in elliptical photonic lattices," Opt. Lett. **33**, 2785–2787 (2008).
24. F. Ye, D. Mihalache, and B. Hu, "Elliptic vortices in composite Mathieu lattices," Phys. Rev. A **79**, 053852 (2009).
25. B. M. Rodríguez-Lara and R. Jáuregui, "Dynamical constants for electromagnetic fields with elliptic-cylindrical symmetry," Phys. Rev. A **78**, 033813 (2008).
26. J. C. Gutiérrez-Vega, M. D. Iturbe-Castillo, G. A. Ramírez, E. Tepichín, R. M. Rodríguez-Dagnino, S. Chávez-Cerda, and G. H. C. New, "Experimental demonstration of optical Mathieu beams," Opt. Commun. **195**, 35–40 (2001).
27. S. Chávez-Cerda, M. J. Padgett, I. Allison, G. H. C. New, J. C. Gutiérrez-Vega, A. T. O'Neil, I. MacVicar, and J. Courtial, "Holographic generation and orbital angular momentum of high-order Mathieu beams," J. Opt. B Quant. Semiclass. Opt. **4**, S52–S57 (2002).
28. C. López-Mariscal, M. A. Bandrés, and J. C. Gutiérrez-Vega, "Observation of the experimental propagation properties of Helmholtz-Gauss beams," Opt. Eng. **45**, 068001 (2006).
29. A. Vasara, J. Turunen, and A. Friberg, "Realization of general nondiffracting beams with computer-generated holograms," J. Opt. Soc. Am. A **6**, 1748–1754 (1989).
30. J. A. Davis, J. Guertin, and D. M. Cottrell, "Diffraction-free beams generated with programmable spatial light modulators," Appl. Opt. **32**, 6368–6370 (1993).
31. V. Arrizón, D. Sánchez-de-la-Llave, U. Ruiz, and G. Méndez, "Efficient generation of an arbitrary nondiffracting Bessel beam employing its phase modulation," Opt. Lett. **34**, 1456–1458 (2009).
32. I. Ricardez-Vargas and K. Volke-Sepúlveda, "Experimental generation and dynamical reconfiguration of different circular optical lattices for applications in atom trapping," J. Opt. Soc. Am. B **27**, 948–955 (2010).
33. G. Indebetouw, "Nondiffracting optical fields: some remarks on their analysis and synthesis," J. Opt. Soc. Am. A **6**, 150–152 (1989).
34. J. Arlt, "Handedness and azimuthal energy flow of optical vortex beams," J. Mod. Opt. **50**, 1573–1580 (2003).